Research article

PDGF-D-induced immunoproteasome activation and cell-cell interactions

Jianing Zhang [a,1], Wanhong Li [a,1], Zhen Xiong [a,1], Juanhua Zhu [a], Xiangrong Ren [a], Shasha Wang [a], Haiqing Kuang [a], Xianchai Lin [a,*], Antonio Mora [b,*], Xuri Li [a,*]

[a] State Key Laboratory of Ophthalmology, Zhongshan Ophthalmic Center, Sun Yat-sen University, Guangzhou 510060, Guangdong, China
[b] Joint School of Life Sciences, Guangzhou Medical University and Guangzhou Institutes of Biomedicine and Health (Chinese Academy of Sciences), Xinzao, Panyu district, Guangzhou 511436, Guangdong, China

ABSTRACT

Platelet-derived growth factor-D (PDGF-D) is abundantly expressed in ocular diseases. Yet, it remains unknown whether and how PDGF-D affects ocular cells or cell-cell interactions in the eye. In this study, using single-cell RNA sequencing (scRNA-seq) and a mouse model of PDGF-D overexpression in retinal pigment epithelial (RPE) cells, we found that PDGF-D overexpression markedly upregulated the key immunoproteasome genes, leading to increased antigen processing/presentation capacity of RPE cells. Also, more than 6.5-fold ligand-receptor pairs were found in the PDGF-D overexpressing RPE-choroid tissues, suggesting markedly increased cell-cell interactions. Moreover, in the PDGF-D-overexpressing tissues, a unique cell population with a transcriptomic profile of both stromal cells and antigen-presenting RPE cells was detected, suggesting PDGF-D-induced epithelial-mesenchymal transition of RPE cells. Importantly, administration of ONX-0914, an immunoproteasome inhibitor, suppressed choroidal neovascularization (CNV) in a mouse CNV model *in vivo*. Together, we show that overexpression of PDGF-D increased pro-angiogenic immunoproteasome activities, and inhibiting immunoproteasome pathway may have therapeutic value for the treatment of neovascular diseases.

1. Introduction

Retinal pigmental epithelial (RPE) cells consist of a monolayer membrane of pigmented cells between the retina and the choroid in the back of the eye. RPE cells are crucial for the normal functions of the eye and form a protective barrier to maintain the ocular immune privilege. The immune-regulatory function of RPE cells plays a pivotal role in retinal immunity, infection and degeneration [1–3]. RPE cells modulate retinal immunity by regulating antigen presentation, activating complement pathways and various signaling molecules, and producing different cytokines [4]. RPE dysfunction is associated with numerous blinding diseases, such as age-related macular degeneration (AMD) and proliferative vitreoretinopathy (PVR) [5,6]. Different mechanisms play a part in RPE-associated pathogenesis, such as aging, inflammation, the accumulation of misfolded proteins, impairment of tight junctions of RPE, and the dysregulation of various signaling pathways [7–10].

PDGF-D is relatively new in the PDGF family and is known to be centrally involved in angiogenesis, cell proliferation and migration, tissue repair and regeneration, and fibrosis formation [11–19]. PDGF-D deregulation was observed in many ocular diseases [13,15,20], and has been shown to be associated with the prognosis of different tumors [21–24]. PDGF-D is upregulated in choroidal neovascularization (CNV), and *Pdgf-d* knockdown in mice inhibited CNV [14]. We have previously shown that PDGF-D activates the complement pathway, and blocking C3a/C3aR activity mitigated PDGF-D-induced CNV [25]. However, it remains unclear whether PDGF-D affected

immune cells in the RPE-choroid complex in the eye, particularly, at a single cell level.

To this end, we conducted single-cell RNA sequencing (scRNA-seq) using mouse RPE-choroid tissues with AAV-induced PDGF-D overexpression in RPE cells, and investigated the impact of PDGF-D on RPE and other cells. Our results revealed that PDGF-D induced the activation of immunoproteasomes, which appeared to be a common response shared by RPE, stromal and immune cells. Increased PDGF-D expression also significantly promoted cell-cell interactions between RPE cells and recruited inflammatory cells. Moreover, administration of an immunoproteasome inhibitor markedly reduced PDGF-D-induced CNV *in vivo*. Our study provides new insights into the molecular understanding of the complex cell-cell interactions induced by PDGF-D in the development of an inflammatory milieu in the eye, and inhibiting immunoproteasome might be a clinically promising strategy for the treatment of inflammatory neovascular diseases.

2. Results

2.1. PDGF-D induces immunoproteasome and IFN-γ signaling in RPE and stromal cells

To explore the cellular targets of PDGF-D, we performed scRNA-seq using mouse RPE-choroid tissues with AAV-mediated PDGF-D overexpression in RPE cells using AAV-GFP as a control (AAV-PDGF-D or AAV-GFP samples hereafter). After unsupervised clustering and annotation using known cell markers (Supplementary Figure 1A), we identified eight cell types in the RPE-choroids: RPE cells, stromal cells, microglia/macrophages (Mig/Mac), dendritic cells (DCs), B cells, nature killer (NK) cells, CD4$^+$ T cells and CD8$^+$ T cells (Fig. 1A, Supplementary Table S.1).

Importantly, the immune cells were mostly detected in the AAV-PDGF-D samples, while the RPE cells, stromal cells, and microglia/macrophages were identified in both AAV-PDGF-D and AAV-GFP samples (Supplementary Figure 1B). Moreover, the proportion of RPE cells was significantly lower and the proportions of stromal cells and microglia/macrophages were markedly higher in the AAV-PDGF-D samples (Supplementary Figure 1C). In addition, gene set enrichment analysis (GSEA) of the RNA-seq results (GSE164972) showed that the immune cell signatures positively correlated with PDGF-D overexpression, while the retinal cell signatures negatively correlated with PDGF-D overexpression at a tissue-level (Supplementary Figure 1D,E, Supplementary Table S2).

PDGF-D mainly binds to *Pdgfr-β* [26]. The expression of *Pdgfr-β* and *Pdgfr-α* were mostly detected in RPE and stromal cells (Fig. 1B). In RPE cells, only *Pdgfr-β* expression was detected, while both *Pdgfr-β* and *Pdgfr-α* expression were observed in stromal cells (Fig. 1B). PDGF-D overexpression decreased *Pdgfr-β* expression in RPE cells (Fig. 1B). Forty-four genes were upregulated and four genes downregulated in the PDGF-D-overexpressing RPE cells, stromal cells and RPE-choroid complex (Fig. 1C). The differentially expressed genes were consistent in RPE, stromal cells, and RPE-choroids, and the changes in gene expression observed in RPE-choroids reflected the changes in RPE and stromal cells respectively (Fig. 1D).

Noteworthy, functional enrichment analysis of the single cell RNA sequencing data suggested that the biological functions of the genes differently expressed were mainly related to antigen processing/presentation and IFN-γ signaling (Fig. 1E). The key genes encoding the catalytic subunits of immunoproteasome, namely *Psmb8, -9* and *-10*, were identified in the enriched antigen-processing and presentation biological processes (Fig. 1E, Supplementary Table S3). The immunoproteasome is a specialized proteasome isoform, which facilitates the processing and presentation of peptides of class I molecules [27]. Functional enrichment analysis of the differentially expressed genes showed that the upregulated genes found in PDGF-

D-overexpressing RPE cells were mostly involved in immunoregulation processes, such as processes involving cellular chemical homeostasis and the differentiation of lymphocytes and myelocytes (Fig. 1F), while the genes downregulated in stromal cells were mostly involved in blood vessel or muscle tissue development (Fig. 1F). Transcription factor regulation prediction analysis showed that the differentially activated transcription factors in RPE and stromal cells were similar (Supplementary Figure S2A, S2B), including IRF1, IRF2, IRF7 and STAT1, which are related to innate immunoregulation and interferon signaling (Supplementary Figure S2A). Furthermore, real-time PCR validated the upregulation of the key immunoproteasome related genes *Psmb8, -9* and *-10* and the interferon pathway related genes *Ifngr1, Ifngr2* and *Stat1* in the PDGF-D overexpressing RPE-choroids (Fig. 1G,H).

### 2.2. PDGF-D-induced sub-clusters of RPE and stromal cells

Sub-clustering analysis of the single cell RNA-seq data identified two clusters of RPE cells with PDGF-D- or GFP-overexpression (Fig. 2A, AAV-PDGF-D or AAV-GFP). The PDGF-D-overexpressing RPE cells displayed a high level of *Cd74* expression (RPE_Cd74, Fig. 2B,C, Supplementary Table S4), and the GFP-overexpressing RPE cells displayed a high level of *Tmem27* expression (RPE_Tmem27, Fig. 2B,C, Supplementary Table S4). We further performed a linked network analysis using GeneMANIA [28] and found that the genes downregulated in the PDGF-D-overexpressing RPE cells were highly interactive with the RPE markers *Rpe65, Rdh5, Rdh10* and *Kcnj13* (Fig. 2D). Functional enrichment analysis showed that the upregulated genes in the PDGF-D-overexpressing RPE cells were mostly related to the innate immune system, IFN-γ signaling, and antigen processing/presentation (Supplementary Figure S3, Supplementary Table S5).

Sub-clustering analysis of stromal cells revealed four sub-populations, Stroma_Ctgf, Stroma_RPELike, Stroma_Cd74 and Stroma_Pi16 (Fig. 2E-G). PDGF-D overexpression resulted in two unique sub-clusters of stromal cells, Stroma_Cd74 and Stroma_RPELike (Fig. 2G). The Stroma_Cd74 sub-cluster expressed a high level of *Cd74*, and the Stroma_RPELike cluster expressed a high level of RPE markers, such as *Rpe65, Rdh5* and *Kcnj13* (Fig. 2G). A cluster-specific functional enrichment analysis showed that the Stroma_Cd74 sub-cluster was specifically related to the regulation of innate immunity (Fig. 2H), while all the clusters were related to angiogenesis, cell adhesion/migration, development, and cellular fiber and matrix organization (Fig. 2H). Real-time PCR confirmed the upregulation of *Psmb8, -9* and *-10* in the human RPE cells (ARPE-19) and human brain vascular adventitial fibroblasts (hBVAF) after PDGF-D stimulation (Fig. 2I-K).

2.3. Pseudotime analysis suggesting PDGF-D-induced epithelial-mesenchymal transition (EMT) of RPE cells

Given that the two stromal clusters from the PDGF-D-overexpressing samples displayed certain features of RPE cells, we performed a pseudotime analysis of the three clusters, RPE_Cd74, Stroma_Cd74 and Stroma_RPELike, to study their potential relationships. The result displayed a trend of transcriptomic transition among them (Fig. 3A,B). The Stroma_RPELike cluster appeared to be intermediate between the RPE_Cd74 and Stroma_Cd74 clusters (Fig. 3C). Pseudotime gene expression analysis showed that the expression of a series of genes correlated with pseudotime (Fig. 3C-F). The expression of the genes related to collagen synthesis, such as Col1a2, Col1a1, and Col3a1, increased gradually in pseudotime (Fig. 3C).

We next validated the above observations by immunofluorescence staining of RPE65 (an RPE marker), vimentin and fibronectin (mesenchymal cell markers) using mouse RPE-choroid
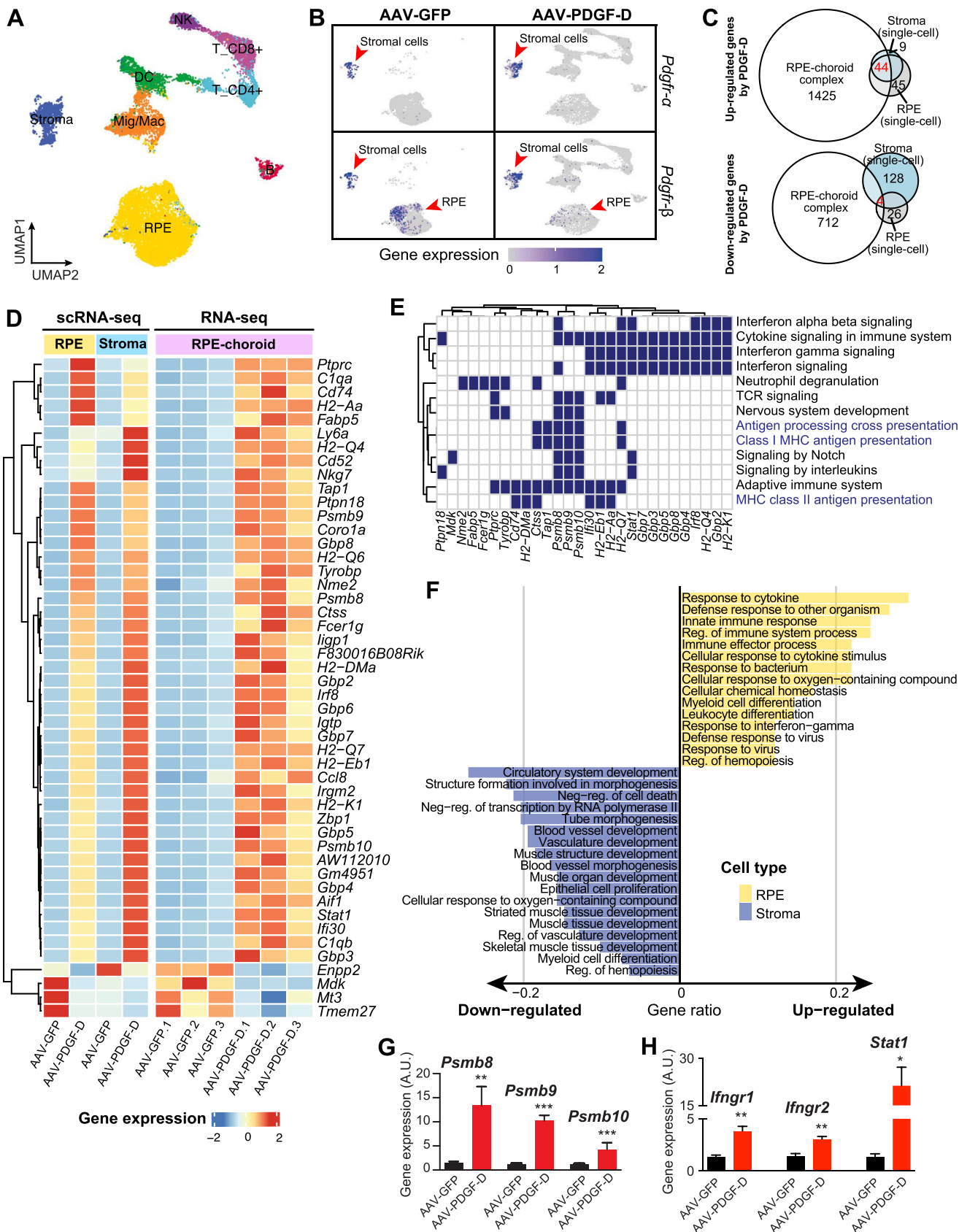
(caption on next page)

Fig. 1. scRNA-seq and bulk RNA-seq analysis show that PDGF-D upregulated immunoproteasome and interferon-dependent pro-inflammatory genes in mouse RPE-choroid complex.
(A) UMAP plot of cell distribution (color-coded by cell types) of all the cells obtained from AAV-GFP- or AAV-PDGF-D-treated mouse RPE-choroids. (B) UMAP plots of *Pdgfr-α* and *Pdgfr-β* expression in mouse RPE-choroids from mice received AAV-GFP or AAV-PDGF-D respectively. (C) Three-way Venn diagrams presenting the unique or overlapping up- or downregulated genes in RPE cells, stromal cells of the RPE-choroid complex with PDGF-D-overexpression in RPE cells. (D) Heatmap of gene expression levels of up- or down-regulated genes in RPE cells, stromal cells or the RPE-choroid complex with PDGF-D-overexpression in RPE cells. Colors represent row-wise scaled gene expression by Z-score. Color scale: red: high expression level, blue: low expression level. (E) REACTOME pathway enrichment result showing the biological processes of the genes up- or downregulated in RPE cells, stromal cells and RPE-choroid complex with PDGF-D-overexpression in RPE cells. (F) Bar plot of top Gene Ontology (GO) pathways enriched in the differentially expressed genes from the RPE and stromal cells of RPE-choroids received AAV-PDGF-D. Reg: regulation. (G,H) Real-time PCR validation of the expression of the key immunoproteasome genes *Psmb8*, *Psmb9* and *Psmb10* (G) and the IFN-γ signaling pathway genes *Ifngr1*, *Ifngr2* and *Stat1* (H) in the mouse RPE-choroids received AAV-GFP or AAV-PDGF-D. n = 4 per group. All error bars indicate SEM. $*P < 0.05$, $**P < 0.01$, $***P < 0.001$. Unpaired student's test was used.

sections (Fig. 3G,H). We found that in the PDGF-D overexpressing RPE cells, more co-staining of RPE65 with vimentin or fibronectin was found (Fig. 3G,H), suggesting EMT of the RPE cells over-expressing PDGF-D, consistent with the pseudotime analysis. Additionally, the expression of the melanin synthesis genes *Tyrp1*, *Dct*, and *Mlana* decreased in the RPE cells overexpressing PDGF-D (Fig. 3I). Consistently, H&E staining confirmed these findings by showing a de-colored RPE layer in the PDGF-D-overexpressing samples (Fig. 3J).

2.4. PDGF-D's-induced cell communications

It remains not well understood currently whether and how PDGF-D affects cell-cell interactions in the RPE-choroid complex. To this end, we performed a ligand-receptor analysis of the single cell dataset using CellChat [29]. We found more than 6.5-fold more li-gand-receptor pairs in the PDGF-D overexpressing RPE-choroids than in the control ones (Fig. 4A), suggesting increased cell-cell communications. We found that the connections among different cell types in the PDGF-D-overexpressing tissues were more complex with more cell types involved, while the connections among cell types in the GFP-overexpressing samples were simpler and mainly between the Stroma_Ctgf and RPE_Tmem27 clusters (Fig. 4B). Moreover, the PDGF pathways appeared to mainly target stromal cells (Fig. 4C, Supplementary Figure S4A). The strongest connection of *Pdgf-d-Pdgfr-β* was observed between the RPE_Cd74 and Stro-ma_Cd74 clusters (Fig. 4C). Intercellular functional interaction ana-lysis revealed cross-cellular PDGF pathway communications among Stroma_RPELike, Stroma_Cd74 and Stroma_Pi16 clusters (Supple-mentary Figure S4A). The PDGF pathway connections among Stro-ma_RPELike and other stromal clusters were similar to those of RPE_Cd74 (Supplementary Figure S4A). The similar pathway con-nectivities between the Stroma_RPELike and the RPE_Cd74 clusters suggested that the Stroma_RPELike cells might be derived from the RPE_Cd74 cells.

In addition, the complement pathways targeting NK cells and microglia/macrophages were activated in the PDGF-D-over-expressing tissues (Fig. 4D). All the three stromal clusters (Stro-ma_Cd74, Stroma_RPELike, and Stroma_Pi16) and the RPE cluster (RPE_Cd74) in the PDGF-D-overexpressing tissues displayed con-nections with the complement pathways targeting NK cells and microglia/macrophages (Fig. 4D). The connections of the stromal clusters were stronger than those of the RPE cluster (Fig. 4D). These data suggested that the stromal cells responding to PDGF-D stimu-lation or the stromal cells derived from transformed RPE cells were the major contributors to the activation of the complement path-ways. In the AAV-PDGF-D RPE-choroids, the RPE cells appeared to be connected with NK cells, CD8+ T cells and microglia/macrophages via various pathways, such as the Madcam1-(Itga4 +Itgb7) pathway and the Mif-(CD74Cd44/Cd74 +Cxcr4)/Ackr3 pathway (Fig. 4E-H). Ad-ditionally, the stromal and RPE cells in the PDGF-D overexpressing RPE-choroids displayed connections to chemokine pathways, such as the Cxcl9/Cxcl10-Cxcr3 pathway and the Ccl5/Ccr5 pathway (Sup-plementary Figure S4B). They are also connected to the MHC mo-lecules, such as H2-d1-Cd8a and H2-t23-(Klrd1 +Klrc1) (Fig. 4I,J).

Cells in the Stroma_Pi16 cluster exhibited strong connections to the RPE_Cd74 and Stroma_RPELike clusters but weak connections to the Stroma_Cd74 cluster in terms of the Igf1-Igf1r or Tnxb-Sdc4 path-ways (Supplementary Figure S4C). Several known ligand-receptor pairs between RPE and stromal cells/microglia that function to maintain cell survival [30,31], such as the Jam3-(Itgam+Itgb2) and the Ctf1-(Lifr+Il6st) ligand-receptor pairs, were inactivated in the PDGF-D-overexpressing RPE-choroids (Supplementary Figure S4D).

### 2.5. Target molecules of PDGF-D and PDGFR-β in the human RPE gene correlation network

PDGFR-β is a major receptor for PDGF-D [26]. We therefore analyzed *PDGFR-β* expression in human eye tissues using the public dataset from eyeIntegration [32]. We found that RPE cells displayed the highest *PDGFR-β* expression compared to cornea and retina (Fig. 5A). A themed functional enrichment analysis was conducted using 692 genes related to *PDGFR-β* in human RPE cells according to eyeIntegration [32] (Fig. 5B). The enriched functional network dis-played four major biological aspects, including the regulation of vascular function, immune cells, development and extracellular matrix (Fig. 5C). Interestingly, most *PDGFR-β* target genes displayed changes in expression in the PDGF-D-overexpressing RPE-choroids (Fig. 5D). In addition, we found that the genes involved in the complement pathways, *C1ra*, *C1s1*, *C4b* and *C3*, were upregulated in the PDGF-D-overexpressing RPE cells (Fig. 5E).

2.6. Inhibition of immunoproteasome ameliorates pathological neovascularization and inflammation in vivo

Overexpression of PDGF-D upregulated the expression of im-munoproteasome genes not only in RPE and stromal cells (Fig. 1C), but also in immune cells as well, particularly, in microglia/macro-phages, DC and B cells (Supplementary Figure S5), all of which play important roles in inflammatory neovascularization [1]. We there-fore hypothesized that immunoproteasome may be an important target in inflammatory neovascularization. In a laser-induced mouse CNV model, the expression of *Pdgf-d*, *Psmb8* and *-10* was significantly upregulated in the RPE-choroid tissues with CNV (Fig. 6A,B). We next examined whether blocking immunoproteasome could suppress neovascularization in the laser-induced mouse CNV model using a known immunoproteasome inhibitor ONX-0914 (PR-957) that tar-gets LMP7 (ß5i, encoded by *Psmb8*) and LMP2 (ß1i, encoded by *Psmb9*) of the immunoproteasome [33]. Intraperitoneal injection of ONX-0914 significantly reduced IB4+ CNV areas and infiltration of microglia/macrophage, especially, in the mouse eyes with PDGF-D overexpression (IBA1+, Fig. 6C).

3. Discussion

To dissect the cell-cell interactions and transcriptomic alterations in choroidal inflammatory neovascularization induced by PDGF-D, we used a single-cell transcriptome sequencing approach and ana-lyzed the RPE-choroids from mice with PDGF-D over-expression in RPE cells. We investigated the alterations of cellular components and
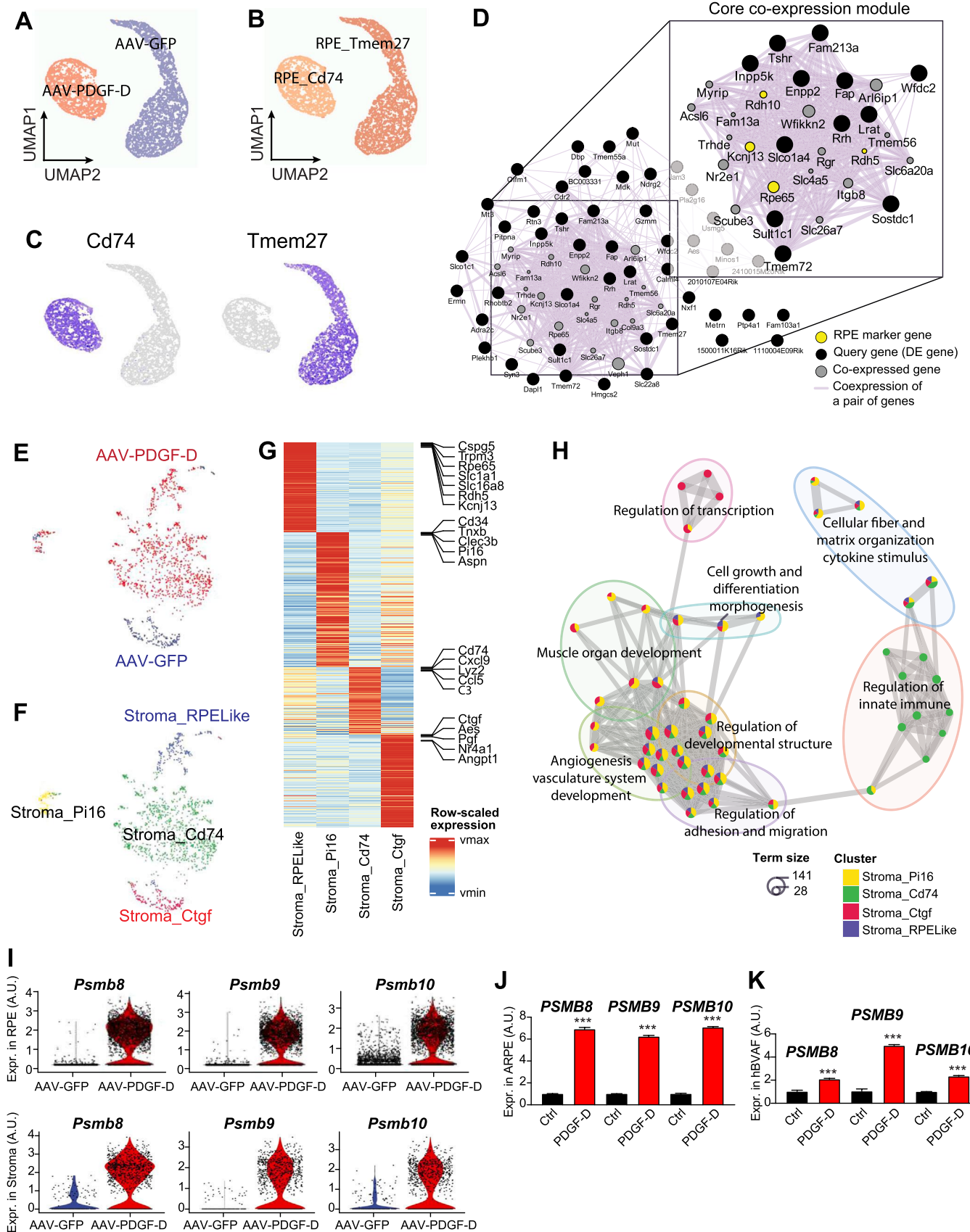
(caption on next page)

Fig. 2. PDGF-D promotes the expression of genes involved in antigen presentation of RPE and stromal cells.
(A,B) UMAP plots of RPE cells color-coded for experimental treatment (A) and subclusters (B) respectively. (C) UMAP visualization of the expression of the RPE subcluster markers *Cd74* and *Tmem27* in the RPE subpopulations. (D) The sub-network of the downregulated genes in RPE cells induced by PDGF-D overexpression and the core connected genes in the gene-gene co-expression network. (E,F) UMAP visualization of stromal cells color-coded for experimental treatment (E) and subclusters (F), respectively. (G) Heatmap of gene expression levels of stromal subcluster marker genes with the top five uniquely expressed genes and the RPE marker genes highlighted by short horizontal lines. (H) Network plot of enriched biological functions of the stromal subcluster marker genes. Colored pie nodes represent enriched biological functions. The nodes inside the translucent circle represent similar biological functions shared. (I) Violin plots of expression of the immunoproteasome genes *Psmb8*, *-9* and *-10* in RPE and stromal cells. (J,K) Real-time PCR validation of gene expression of *PSMB8*, *-9* and *-10* in ARPE-19 cells (J) or hBVAF cells (K) with or without PDGF-D treatment. n = 3 each group. All error bars indicate SEM. Unpaired student's test was used. * $P < 0.05$, ** $P < 0.01$, *** $P < 0.001$.

the changes of molecular signatures induced by PDGF-D at both cell and tissue levels.

RPE cells function as antigen-presenting cells [34]. Our study showed that PDGF-D overexpression in RPE cells upregulated the expression of many key immunoproteasome genes, such as *Psmb8*, *-9* and *-10*, in both RPE and a subgroup of stromal cells (Fig. 6D). Immunoproteasome is a special isoform of proteasome containing the catalytic subunits that can largely replace the catalytic parts of canonical proteasomes upon inflammatory cytokine stimulation or virus infection [27,35]. *Psmb8*, *Psmb-9*, *Psmb-10*, *Cd74* and *Ctss* are key genes involved in antigen processing and presentation [36–40]. Inhibition of immunoproteasome suppresses antigen presentation and T and B cell activation [36–38]. In the retina, immunoproteasome deficiency in RPE cells protected retinae from apoptosis [41]. In addition, infiltrated immune cells also express high levels of immunoproteasome genes [35]. In this work, we observed that immunoproteasome genes were highly expressed in both tissue and immune cells in the PDGF-D-overexpressing RPE-choroid complex. Immunoproteasomes promote the production of antigen epitopes, which regulate the immune responses of cells [27]. As such, inhibition of immunoproteasome activity can simultaneously suppress immune responses of immune cells and tissue resident cells, and can prevent further recruitment of immune cells from the circulatory system [36].

We further found that overexpression of PDGF-D may have induced epithelial-mesenchymal transition (EMT) of RPE cells, since a subgroup of stromal cells expressed key RPE cell markers *Rpe65*, *Rdh10* and *Rdh5*. As specialized epithelial cells, RPE cells undergo EMT in a variety of diseases [42,43]. Studies have shown that RPE cells display a high level of plasticity in pathological processes [5]. Transition of RPE cells towards a mesenchymal phenotype could be related to the down-regulation of the RPE-related genes *Rpe65*, *Cdh10* and *Cdh5* and the upregulation of mesenchymal genes *Vim* and *Fn1* [44,45]. Indeed, in this work, co-immunofluorescence staining of mesenchymal cell markers vimentin or fibronectin together with the RPE marker RPE65 showed that PDGF-D overexpression induced the expression of mesenchymal markers in RPE cells.

It is interesting that PDGF-D-overexpression resulted in three unique clusters, the RPE_Cd74, Stroma_Cd74, and Stroma_RPELike clusters, all of which contained predominantly PDGF-D-overexpressing cells. Both the RPE_Cd74 and the Stroma_Cd74 clusters displayed a high level of Cd74 expression. CD74 is known as an HLA class II histocompatibility antigen gamma chain, and plays an important role in antigen presentation by functioning as a chaperone for MHC class II molecules [38–40]. Our findings indicate that PDGF-D-overexpression in RPE cells increased the antigen processing and presentation properties in both RPE and stromal cells. The Stroma_RPELike cluster, however, displayed RPE properties since they expressed high levels of RPE markers, such as *Rpe65*, *Rdh5* and *Kcnj13*. The Stroma_Pi16 cluster with a high level of *Pi16* expression was found in both the PDGF-D-overexpressing and the control samples. Pi16 is a pan-tissue marker of fibroblasts [46].

Our data showed that PDGF-D overexpression markedly increased cell-cell interactions in the choroids, particularly, the interplay between choroidal and immune cells via various pathways. Pathways related to antigen presentation and inflammatory

responses [39], such as the Mif-(CD74 +Cd44/Cd74 +Cxcr4) pathway, connect the RPE_Cd74 and Stroma_RPELike cells to NK, T, and B cells and microglia/macrophages. In addition, complement pathways, such as the C3-(Itgam/Itgax+Itgb2) pathway, were observed among the AAV-PDGF-D-specific stromal clusters, microglia/macrophages and NK cells, suggesting that the stromal clusters induced by PDGF-D overexpression may regulate the activation of complement pathways [25,47]. The potential cellular interplay among other cell types, such as among ECs and other choroidal cells still requires further study.

Moreover, our study demonstrated that immunoproteasome is a crucial downstream target of PDGF-D in choroidal neovascularization. In a laser-induced mouse CNV model, the expression levels of *Pdgf-d* and the key immunoproteasome genes increased in RPE-choroids, and PDGF-D over-expression in RPE cells exacerbated laser-induced choroidal neovascularization. Importantly, administration of ONX-0914, an immunoproteasome inhibitor [33], reduced inflammation and angiogenesis in a mouse CNV model, supporting that immunoproteasome may be a promising target in PDGF-D-induced inflammatory neovascularization.

In summary, in this study, we reveal that RPE-specific PDGF-D overexpression in mice upregulated the expression of immunoproteasome genes in different cell types, including RPE cells, stromal cells, microglia/macrophages, and other immune cells. PDGF-D overexpression also increased EMT and antigen presentation of RPE cells. The close association of immunoproteasome with PDGF-D overexpression and inflammatory angiogenesis suggests that immunoproteasome may be an important target in inhibiting PDGF-D-induced pathological neovascularization and inflammation.

4. Materials and methods

4.1. Animals

All experiments using mice were approved by the Animal Care and Use Committee of Sun Yat-sen University, People's Republic of China. C57BL/6 J (6–8 weeks old) mice were purchased from Beijing Vital River Laboratory Animal Technology Co., Ltd., China. All mice were housed in an SPF facility in the Ophthalmic Animal Laboratory of Zhongshan Ophthalmic Center at the Sun Yat-sen University and maintained on a 12/12 h light/dark cycle with water and chow provided *ad libitum*.

Euthanasia of mice was performed according to the guidelines from the American Veterinary Medical Association (https://www.avma.org/KB/Policies/Documents/euthanasia.pdf) and the National Institutes of Health in USA (http://grants.nih.gov/grants/olaw/120301_seminar_transcript.pdf). Briefly, carbon dioxide (CO_2) inhalation was used followed by cervical dislocation for death confirmation of mice. The death of mice was induced as painlessly and quickly as possible by trained personnel and compressed CO_2 gas in cylinders was used as it allowed the inflow of gas to the induction chamber in a controlled manner.

5. Cell lines and culture conditions

The human ARPE-19 RPE cells (Abnova, ZQ0460) and hBVAF primary human fibroblasts (Sciencell, 1110) were used in this study.
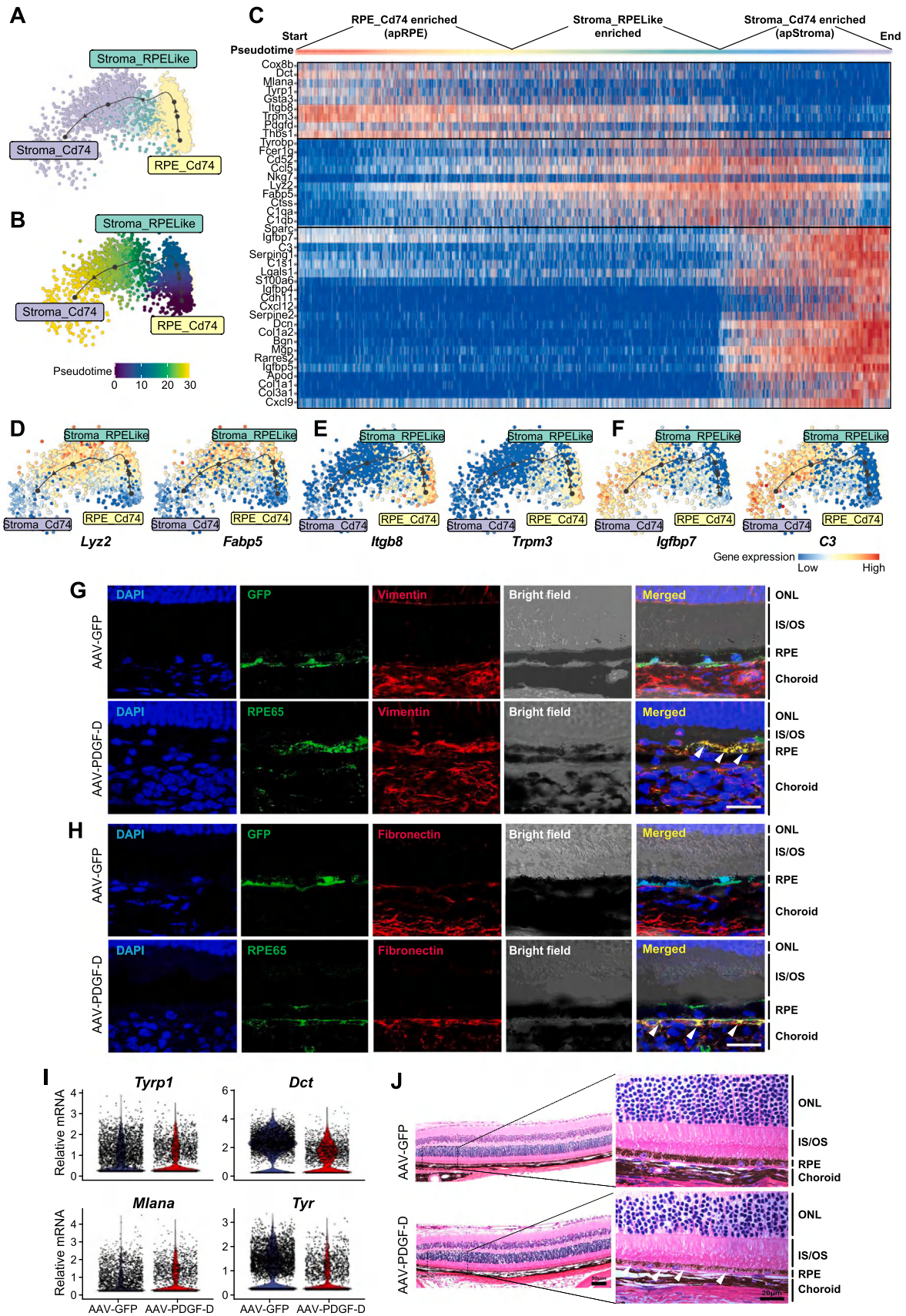
(caption on next page)

Fig. 3. Single-cell pseudotime analysis indicating epithelial mesenchymal transition of RPE cells with PDGF-D overexpression.
(A,B) Pseudotime trajectory of cells from RPE_Cd74, Stroma_RPELike and Stroma_Cd74 clusters colored by cell subclusters (A) or pseudotime (B). (C) Heatmap of expression levels of the genes most significantly changed in pseudotime with the cells in the heatmap ordered by pseudotime value. Blue: low expression level, red: high expression level. (D-F) Expression levels of the genes significantly changed in pseudotime with expression peaks enriched in the Stroma_RPELike cluster (D), RPE_Cd74 cluster (E) and Stroma_Cd74 cluster (F), respectively. (G,H) Immunofluorescence staining of vimentin (G) or fibronectin (H) in RPE cells with or without PDGF-D overexpression in RPE cells. Co-localization is indicated by the white arrows. (I) Violin plots of expression levels of the melanin synthesis genes related to pseudotime in RPE cells. (J) Representative images of hematoxylin-eosin staining of mouse RPE-choroid complex showing less pigmentation in RPE cells overexpressing PDGF-D (white arrows). Scale bar: 50 μm.

The ARPE-19 cells were cultured in tissue culture dishes in DMEM/F12 medium (Gibco, C11330) supplemented with 10% FBS and 1% penicillin/streptomycin (Sciencell, 0503). Passage numbers of the ARPE-19 cells used in our study were from P23 to P29, similar to passage numbers used by other laboratories [48,49]. The hBVAF cells were cultured in tissue culture dishes in fibroblast medium (Sciencell, 2301) supplemented with 2% FBS (Sciencell, 0010), 1% FGS (Sciencell, 2352) and 1% penicillin/streptomycin (Sciencell, 0503). To validate the downstream targets of PDGF-D, the cells were treated with 50 ng/ml of PDGF-D (R&D, 1159-SB-025/CF) or BSA for 6, 12 or 24 h and then harvested for analysis.

5.1. Construction of adeno-associated virus (AAV) for RPE-specific gene expression

The RPE-specific AAV constructs were made as described previously [25]. Briefly, we replaced the CMV promoter of the AAV vector pAV-CMV-C-FH (Vigenebio, China, pAV100001–OE) with the human VMD2 promoter (−598–378 bp from the transcription start site), which drives RPE-specific transgene expression [50]. We replaced the multi-cloning site of the vector with the coding sequence of the human PDGF-D gene or the GFP gene as a control.

6. Sub-retinal injection of AAV vectors in mice

The pupils of 8-week old female mice were dilated by topical application of tropicamide with an intraperitoneal injection of 1% sodium pentobarbital (10 ml/kg body weight) for anesthesia. Procainamide was applied to the cornea for topical anesthesia and carboxymethyl cellulose sodium was used to avoid the development of cornea xerosis. Sub-retinal injection was performed as described previously [25]. Sub-retinal injection of AAV (1 μl/eye, 5×10^{13} vg/ml) was performed via a puncture hole (0.2 mm in diameter) behind the cornea limbus using a sterilized 5 μl syringe (Hamilton, 7633–01) and a 33-gauge blunt needle (Hamilton, 7803–05). Successful injections were indicated by the microscopic or fundus imaging observation of the semicircular retinal detachment around the injection site.

7. Preparation of single cells for single-cell RNA sequencing

To isolate viable single cells from RPE-choroid tissues for single-cell RNA sequencing, the mice treated with AAV-PDGF-D or AAV-GFP four weeks after sub-retinal injection were euthanized and one eye was enucleated. The eye was cleaned from extraocular tissues, and a circumferential incision was performed around the cornea limbus to remove the anterior segments, including the cornea, lens, iris and the ciliary body. The retinae were carefully separated from the choroids and the RPE-choroid complex was cut into eight petals. The RPE-choroidal tissues were digested at 37 °C for 15 min using 200 μl of solution containing 52 U/ml papain (Worthington, LS003126) and 3 mg/ml of DNase I (BioFroxx, 1121MG010). The single cell suspensions were pipetted up and down several times using a 200 μl pipette and filtered through a 45 μm cell strainers.

8. Single-cell RNA sequencing

The library preparation, RNA sequencing, and raw data processing were performed at Berry Genomics (Beijing, China). scRNA-seq libraries were prepared according to 10x Genomics specifications (Single Cell Reagent Kits v3 User Guide, 10x Genomics). Cell suspensions were loaded onto the 10x Genomics chromium platform to generate barcoded single-cell gel bead-in-emulsion (GEMs), targeting ~5000 single cells per sample. GEM-reverse transcription was performed and the cDNA was amplified to generate the libraries. The quality of the cDNA was assessed using the company's standard pipeline. Libraries were quantified using Qubit fluorometric quantification (Thermo Fisher Scientific). Libraries were sequenced using an Illumina HiSeq6000 with paired-end 150 bp reads.

9. Immunofluorescence staining

For immunofluorescence staining, the fixed eyeball Section (15 μm) were incubated in 0.5% Triton X-100 (Sigma, X100) prepared in phosphate buffered saline for 15 min for permeabilization, and then blocked using 5% normal goat serum for 1 h followed by overnight incubation with the primary antibody at 4 °C. The primary antibodies used were: anti-vimentin (Abcam, ab92547), anti-fibronectin (Sigma, F3648), anti-RPE65 (Abcam, ab13826) and anti-IBA1 (WAKO, 019–19741). The slides were washed and incubated for one hour at room temperature with the secondary antibodies (Invitrogen) followed by a 10-minute incubation for DAPI staining (Sigma, D9542). Blood vessels were labeled with I-isolectin B4 (IB4, Thermo Fisher, 121411). The sections were imaged using a Zeiss LSM710 laser-scanning confocal microscope and analysed using ZEN 2012 (Zeiss) and ImageJ.

10. Hematoxylin-eosin (H&E) staining

For H&E staining, RPE-choroid Section (4 μm) were de-waxed as the following: Xylene I (SCRC,10023418) for 20 min, Xylene II (SCRC,10023418) for 20 min, 100% ethanol I (SCRC, 100092683) for 5 min, 100% ethanol II (SCRC, 100092683) for 5 min, and 75% ethanol for 5 min. The sections were stained with hematoxylin solution (Servicebio, G1003) for 3–5 min, rinsed with tap water, followed by hematoxylin differentiation solution (Servicebio, G1003), and then rinsed with tap water. The sections were treated with Hematoxylin Scott Tap Bluing (Servicebio, G1003), and rinsed with tap water. The sections were treated with 85% ethanol for 5 min, 95% ethanol for 5 min followed by eosin dye (Servicebio, G1003) for 5 min. After dehydration, the sections were sealed with neutral gum (SCRC, 10004160). Image acquisition was performed using an AX10 imager Z2 (ZEISS) microscope.

11. Real-time PCR

RNA was isolated using the TRNzol reagent (TIANGEN, DP424) and reverse transcribed using the FastKing First Strand Synthesis kit (TIANGEN, KR116–02). Real-time PCR was performed using 2x color SYBR Green qPCR master mix (EZBioscience, A0012-R2-L). The primers used are listed in Supplementary Table S6. The mean cycle threshold (Ct) value of each sample was analyzed using the 18 S
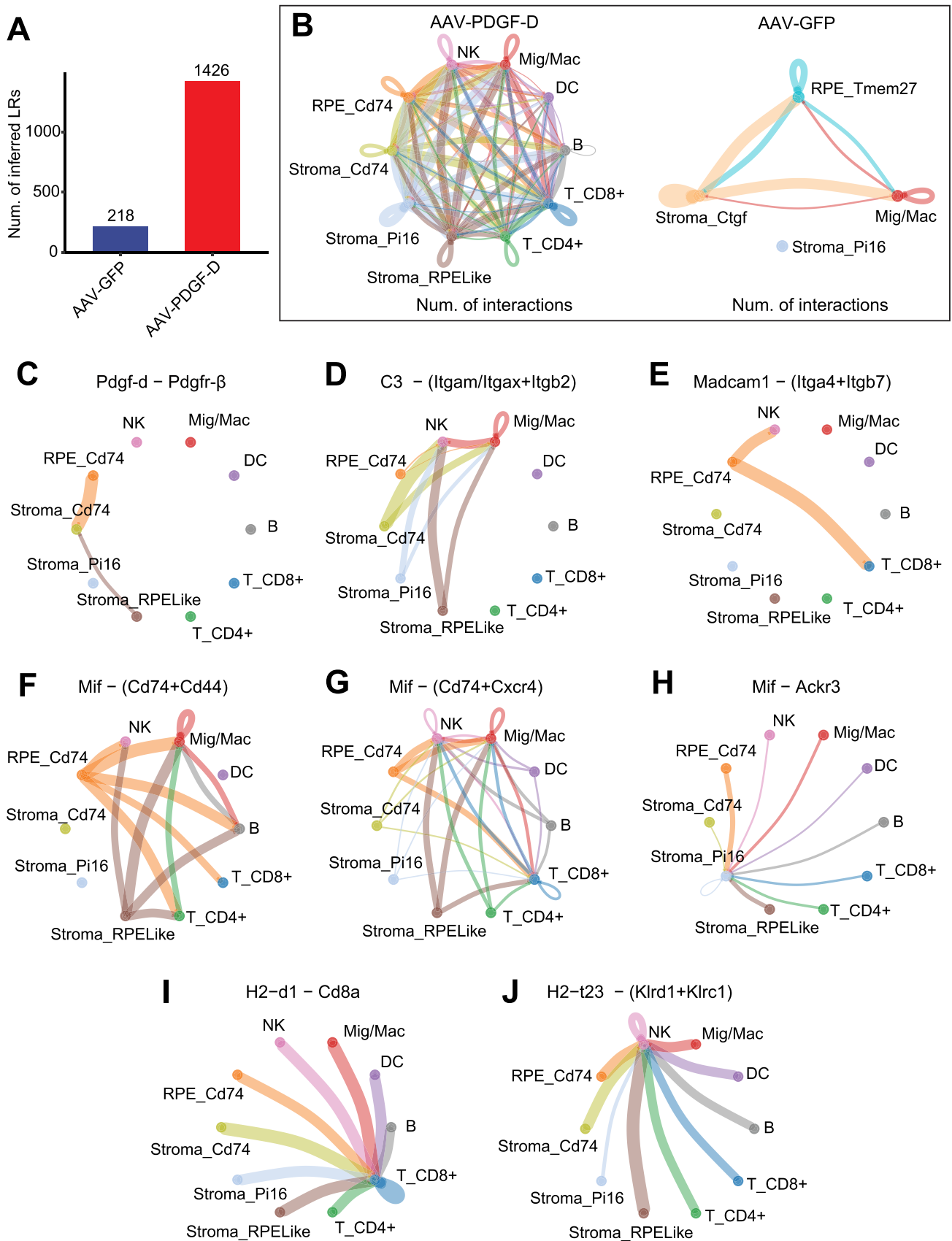
Fig. 4. Cell-cell communications predicted by CellChat in mouse RPE-choroids with PDGF-D overexpression.
(**A**) Bar plot showing the total number of the inferred ligand-receptor interactions in the cells of the RPE-choroids treated with AAV-GFP or AAV-PDGF-D. (**B**) Circle plots showing the roles of the cell subtypes in the cell-cell communications in the RPE-choroids with AAV-PDGF-D or AAV-GFP treatment. (**C-J**) Circular plots displaying the inferred cell interactions of PDGF-D pathway (C), complement pathway (D) and chemotaxis pathway targeting immune cells (E-J), including integrin pathways (E) and MHC antigen presentation pathways (I-J) in the detected cell types in the RPE-choroids received AAV-PDGF-D. The thickness of the lines between cells indicates the strength of the inferred interaction. Node color represents a cell subtype. Edge color represents the cell subtype of the sender.
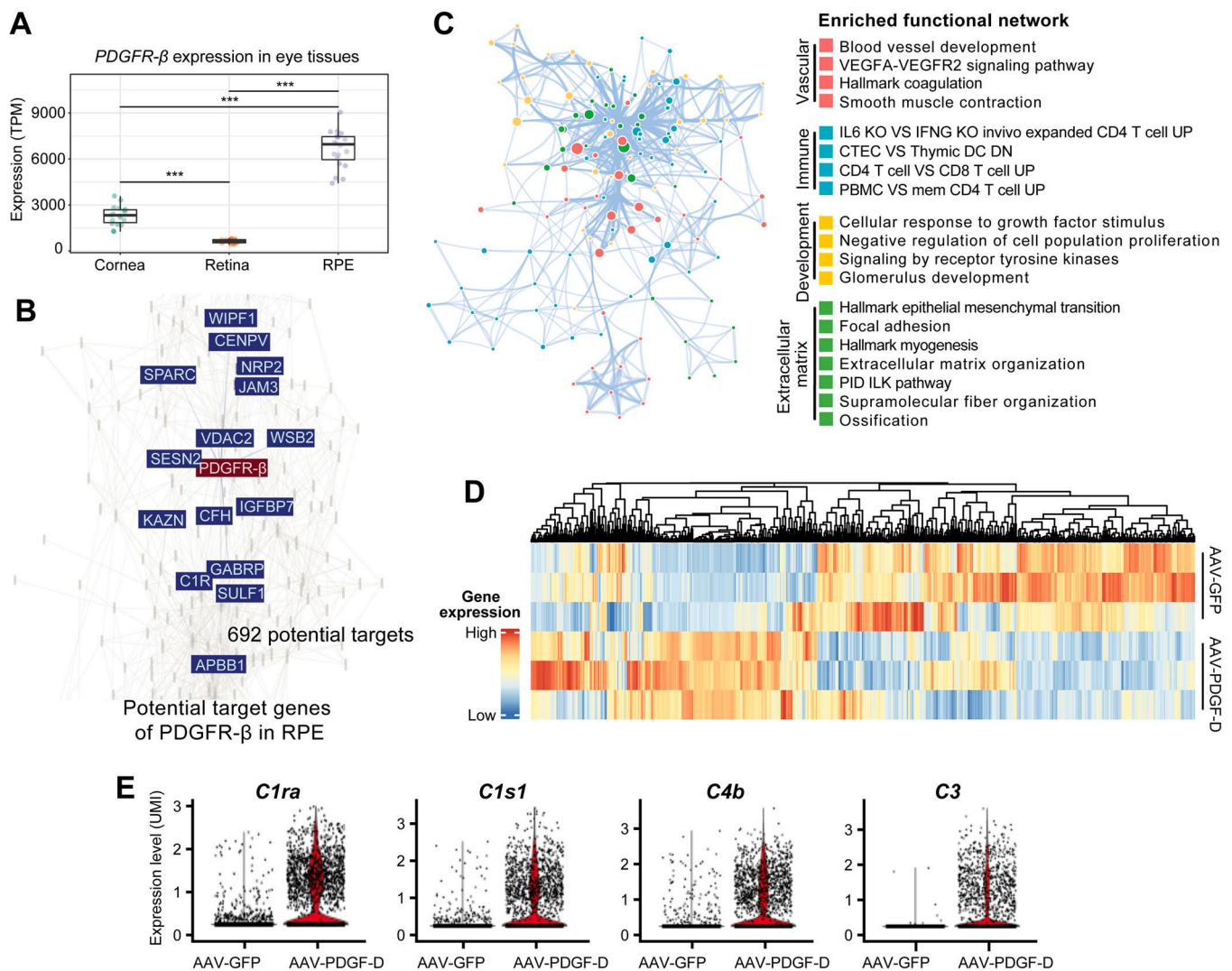
Fig. 5. Genes co-expressed with *PDGFR-β* in the human RPE network.

(A) *PDGFR-β* expression in cornea (n = 18 cornea), retinae (n = 22 retinae) and RPE cells (n = 20 retinal pigment epithelium tissues) using the eye transcriptomic data of adult human tissues from the eyeIntegration database. Error bars indicate SEM. Ordinary one-way ANOVA followed by Turkey's multiple comparison test was used. $^{*} P < 0.05$, $^{**} P < 0.01$, $^{***} P < 0.001$ (B) *PDGFR-β* (red rectangle) and its co-expressed genes (blue rectangle) in the RPE Network. (C) Enriched functional network of *PDGFR-β* and its co-expressed genes in RPE cells. Nodes denote significantly enriched biological processes. Edges denote the membership similarity of the biological processes measured by Metascape. The color of the network node denotes a biological theme. Biological processes with a high degree of membership similarity are assigned to the same biological theme. (D) Heatmap of *Pdgfr-β* expression and its predicted RPE-specific co-expressed genes in mouse RPE-choroid complex treated with AAV-GFP or AAV-PDGF-D. (E) Violin plots showing the upregulation of complement pathway genes co-expressed with *PDGFR-β* in the *PDGF-D* overexpressing RPE cells.

rRNA as a reference, and the result were presented as fold change of the samples. Prism (version 8) was used for analysis.

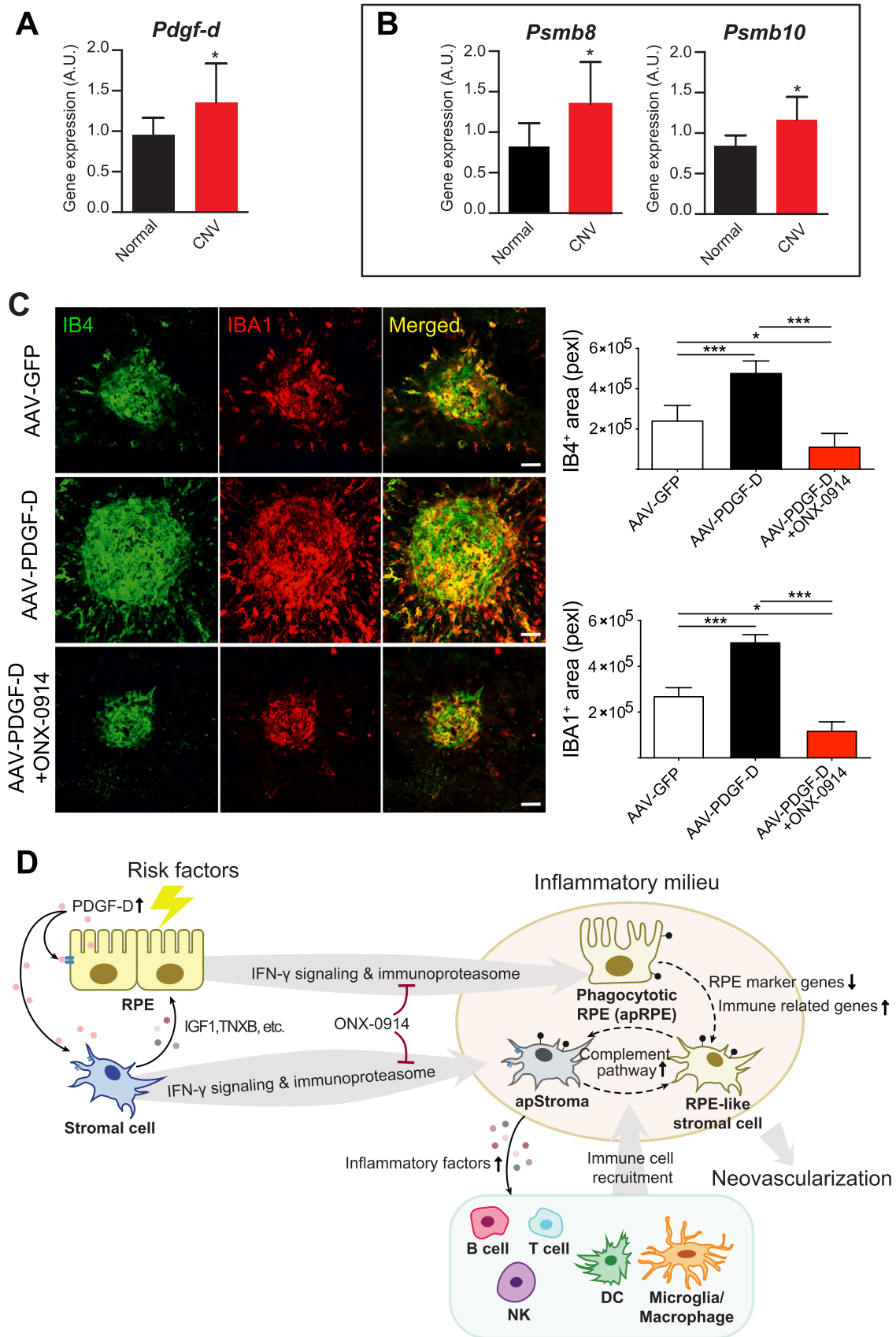## 12. Laser-induced mouse CNV model

The laser-induced mouse CNV model was described previously [51]. Briefly, two weeks after AAV injection, mice were anesthetized, and eyes dilated by topical application of tropicamide. Four laser spots were made by laser injury (90 mV power, 75 ms duration, 75 μm spot size, Oculight Infrared Laser System 810 nm, IRIDEX Corporation) at an equal distance from the optic nerve in each eye to induce CNV. The corneas of the mice were treated with antibiotic tobramycin ointment locally after the laser injury. The mice were then placed on a 37°C electric blanket until fully waking up. Seven days after laser treatment, the eyes were harvested and the eyecups flat-mounted for immunohistochemical staining as described [51].

13. Intraperitoneal injection of immunoproteasome inhibitor

A 100 mg/ml stock solution of the immunoproteasome inhibitor, ONX-0914 (MCE, HY-13207), was prepared by dissolving the compound in sterile dimethyl sulfoxide (DMSO, Sigma, D4540). ONX-0914 was further diluted using corn oil to a final concentration of 1 mg/ml for intraperitoneal injection at a dose of 10 mg/kg body weight. Two weeks after sub-retinal AAV injection, ONX-0914 or vehicle was injected intraperitoneally every 2 days for 3 times in total after laser treatment.

14. Pre-processing and quality control of scRNA-seq data

The Cell Ranger Single Cell Software suite v6.1.0 was used for sample demultiplexing, alignment (reference mouse genome version, refdata-gex-mm10–2020-A), filtering, UMI counting, and quality control using the default parameters. Cells with less than 500 genes detected, or greater than 10% of mitochondrial genes were excluded from the analysis. Genes detected in less than 10 cells were

Fig. 6. ONX-0914, an immunoproteasome inhibitor, suppressed choroid neovascularization and immune cell infiltration *in vivo*.
(A,B) Bar plots of the expression of *Pdgf-d* (A), *Psmb8* and *Psmb10* (B) in RPE-choroids with laser-induced mouse CNV. (C) Immunofluorescence staining and quantitative bar plots of IB4 and IBA1 in laser-induced CNV treated with AAV-GFP, AAV-PDGF-D or AAV-PDGF-D+ONX-0914. AAV-GFP: n = 12 eyes, AAV-PDGF-D: n = 8 eyes, AAV-PDGF-D+ONX-0914: n = 8 eyes. All error bars indicate SEM. Ordinary one-way ANOVA followed by Turkey's multiple comparison test was used. * $P < 0.05$, ** $P < 0.01$, *** $P < 0.001$. (D) Diagram of the complex interplay among RPE, choroidal and immune cells in PDGF-D-induced choroidal inflammatory neovascularization.

also excluded. After data cleaning, 4729 (for AAV-GFP samples) and 11220 (for AAV-PDGF-D samples) cells were sequenced respectively with ~10000 mean reads and a median of ~2000 genes detected per cell. Standard single-cell transcriptome analysis was performed using the Seurat 4.0 R package [52]. Gene expression raw counts were normalized following the default Seurat NormalizeData function with a scale factor of 10000 and a log transformation. Highly variable genes of each dataset were selected by Seurat FindVariableFeatures function (selection.method="mvp", mean.cutoff=c(0.1, Inf)). The initial dim number for PCA analysis was set to 15. PCA components with standard deviation > 1.25 (generated by ElbowPlot) and JackStraw score < 0.05 (generated by ScoreJackStraw) were used to generate two-dimensional UMAP. The same PCA components were used to run the harmony package (version 1.0) [53] to identify common sources of variation between AAV-GFP and AAV-PDGF-D datasets. The new UMAP locations were generated based on the integrated results of harmony, and were used for the downstream cell clustering and visualization. PCA components for RPE sub-clusters and stromal cell sub-clusters were determined using the same strategy used for the integration analysis. The initial PCA dim number for RPE cells and the dim number for stromal cells were both set to 12.

15. Cell clustering and cell type annotation

Unsupervised cell clustering analysis of the integrated single cell dataset was performed using the Seurat 4.0 R package [52]. Cell clustering in the integrated cell population was performed using the FindClusters function. The maximum iterations number was set to 250 for all the cluster analysis. The final resolution of integration datasets, RPE sub-clusters and stromal cell sub-clusters were set to 0.2, 0.8, 0.4, respectively. The cell type annotation for the identified cell clusters in the integrated datasets was determined using the known cell type markers (Supplementary Figure S1A). The names of the sub-clusters within major cell types were determined by the cluster-specific markers (described in the following section) or phenotype-associated features. Clusters without uniquely expressed markers but with biological significance were merged to the nearest clusters determined by the Seurat BuildClusterTree function.

16. Identification of cluster-specific and differently expressed genes

For the scRNA-seq data analysis, the cluster-specific genes were analyzed by the Seurat FindAllMarkers function. The primary markers were further filtered using avg_logFC > 0.5 and pct.1 > 0.5. The differently expressed genes were analyzed using the Seurat FindMarkers function with default parameters and treated with a second filtration: |avg_logFC| > 0.5 and |pct.2-pct.1| > 0.25. Genes meeting the above filtration rules were utilized for downstream functional analysis.

17. Gene set functional analysis

To explore the biological functions of differently expressed gene sets or cell type-specific gene sets, we performed functional enrichment analysis using the clusterProfiler package (version 3.14.3) using four functional annotation databases (GO biological processes, KEGG pathways, Reactome and Biocarta) [54,55]. The minimum gene set size was set to 5 and the maximum set to 1500. Terms were further filtered with the minimum enriched gene number ≥ 3, adjusted P or Q value < 0.05. Gene sets not enriched to any biological terms were used to query the highly functionally interacting gene sets using the integrated mouse gene interaction network provided by GeneMANIA [28] using the default parameters. The extended gene interaction network was visualized using Cytoscape (version 3.7.0) [56].

18. Prediction of cell type- and treatment-specific regulon activities

To estimate the activities of transcription factor regulons in different cell types with different treatments, we used the pySCENIC package (version 0.9.0) using 1675 known transcription factors annotated in RIKEN database and the cisTarget mouse motif v9 annotation [57]. Activities of the regulatory networks were evaluated using the binarized transcription factor regulon score.

18.1. PDGF-D downstream targets prediction in human RPE network

The reference human RPE gene correlation network and the *PDGFR-β*-related genes were downloaded from the eyeIntegration website [32] (https://eyeintegration.nei.nih.gov/). The prediction of biological functions of the related genes was performed using Metascape (https://metascape.org/) [58]. Seven reference databases were used for the enrichment analysis: GO biological processes, Reactome gene sets, KEGG pathway, Immunological signatures, Canonical pathways, Hallmark gene sets and WikiPathways. The themed functional network was visualized by Cytoscape (version 3.7.0) [56].

18.2. Pseudotime analysis of antigen-presenting RPE cells, RPE-like stromal cells and antigen-presenting stromal cells

Pseudotime analysis was performed using the dyno package (version 0.1.2) [59] with cells from the RPE_Cd74, Stroma_RPELike and Stroma_Cd74 clusters from the AAV-PDGF-D samples. Pseudotime was calculated using the Slingshot algorithm wrapped in the dyno package using genes with highly variable expression. The highly variable genes of the selected cells used for pseudotime analysis were re-identified using the Seurat FindVariableFeatures function with a minimum mean value of 1e-5 and an RNA assay data matrix.

19. Cell-cell and ligand-receptor interaction analysis

Cell-cell interaction analysis was performed using CellChat (version 1.1.3) [29]. Since RPE cells and stromal cells can be clearly identified into distinct cell populations in the cell subtype analysis, we applied the labels of cell subsets as the cell labels for CellChat analysis. The mouse CellChat database was used to screen potential ligand-receptor pairs across cell subsets. The default parameters were used for CellChat (https://github.com/sqjin/CellChat). The maximum edge width (edge.width.max) for the visualization of all the circle plots was set to 6.

20. Statistics

The normal distribution of the data was verified using Shapiro-Wilk test before comparisons. For two-group comparisons, statistical analysis was performed using unpaired two-tailed t-test. For multiple-group comparisons, ordinary one-way ANOVA followed by Turkey's multiple comparison test was used. * : $P < 0.05$, ** : $P < 0.01$, *** : $P < 0.001$. Data are presented as mean ± standard error of the mean (SEM).

Conflict of interests

The authors declare that there is no conflict of interest regarding the publication of this article.

Code availability

This study did not generate any unique code.

Funding

CRediT authorship contribution statement

Xuri Li: Conceptualization, Writing – original draft, Writing – review & editing, Project administration, Supervision, Funding acquisition. **Jianing Zhang:** Conceptualization, Methodology, Formal analysis, Investigation, Data curation, Writing – original draft, Writing – review & editing, Visualization, Supervision, Funding acquisition. **Wanhong Li:** Methodology, Formal analysis, Validation, Investigation, Writing – original draft, Writing – review & editing. **Zhen Xiong:** Methodology, Formal analysis, Validation, Investigation, Writing – original draft, Writing – review & editing. **Juanhua Zhu:** Methodology, Formal analysis, Validation, Investigation. **Xiangrong Ren:** Methodology, Resources, Writing – review & editing. **Shasha Wang:** Methodology, Resources, Investigation. **Haiqing Kuang:** Methodology, Resources, Investigation. **Xianchai Lin:** Writing – original draft. **Antonio Mora:** Investigation, Writing – original draft.

Data Availability

The single cell RNA-seq data of mouse RPE-choroid complex treated with AAV-PDGF-D or AAV-GFP were deposited in the Gene Expression Omnibus (GEO, GSE193002). The RNA-seq data of mouse RPE-choroid complex treated with AAV-PDGF-D or AAV-GFP were deposited in the GEO database (GSE164972).

Appendix A. Supporting information

Supplementary data associated with this article can be found in the online version at doi:10.1016/j.csbj.2023.03.047.

References

[1] Taylor AW, Hsu S, Ng TF. The role of retinal pigment epithelial cells in regulation of macrophages/microglial cells in retinal immunobiology. Front Immunol 2021;12:724601.

[2] Storti F, et al. Impaired ABCA1/ABCG1-mediated lipid efflux in the mouse retinal pigment epithelium (RPE) leads to retinal degeneration. Elife 2019:**8**.

[3] Radtke ND, et al. Vision improvement in retinal degeneration patients by implantation of retina together with retinal pigment epithelium. Am J Ophthalmol 2008;146(2):172–82.

[4] Detrick B, Hooks JJ. Klettner AK, Dithmar S, editors. *The RPE Cell and the Immune System*, in *Retinal Pigment Epithelium in Health and Disease*. Cham: Springer International Publishing; 2020. p. 101–14.

[5] Yang S, Zhou J, Li D. Functions and diseases of the retinal pigment epithelium. Front Pharm 2021;12:727870.

[6] Tamiya S, Kaplan HJ. Role of epithelial-mesenchymal transition in proliferative vitreoretinopathy. Exp Eye Res 2016;142:26–31.

[7] Zhong Q, et al. Role of endoplasmic reticulum stress in epithelial-mesenchymal transition of alveolar epithelial cells: effects of misfolded surfactant protein. Am J Respir Cell Mol Biol 2011;45(3):498–509.

[8] Cano M, et al. Oxidative stress induces mitochondrial dysfunction and a protective unfolded protein response in RPE cells. Free Radic Biol Med 2014;69:1–14.

[9] He Y, et al. Mitochondria impairment correlates with increased sensitivity of aging RPE cells to oxidative stress. J Ocul Biol Dis Info 2010;3(3):92–108.

[10] Villarroel M, et al. High glucose concentration leads to differential expression of tight junction proteins in human retinal pigment epithelial cells. Endocrinol Nutr 2009;56(2):53–8.

[11] Li H, et al. PDGF-D is a potent transforming and angiogenic growth factor. Oncogene 2003;22(10):1501–10.

[12] Bergsten E, et al. PDGF-D is a specific, protease-activated ligand for the PDGF beta-receptor. Nat Cell Biol 2001;3(5):512–6.

[13] Ray S, et al. Platelet-derived growth factor D, tissue-specific expression in the eye, and a key role in control of lens epithelial cell proliferation. J Biol Chem 2005;280(9):8494–502.

[14] Kumar A, et al. Platelet-derived growth factor-DD targeting arrests pathological angiogenesis by modulating glycogen synthase kinase-3beta phosphorylation. J Biol Chem 2010;285(20):15500–10.

[15] Kumar A, Li X. PDGF-C and PDGF-D in ocular diseases. Mol Asp Med 2018;62:33–43.

[16] Lee C, Li X. Platelet-derived growth factor-C and -D in the cardiovascular system and diseases. Mol Asp Med 2018;62:12–21.

[17] Aguilar A. Renal fibrosis: PDGF-D in renal fibrosis. Nat Rev Nephrol 2016;12(5):257.

[18] Borkham-Kamphorst E, et al. Pro-fibrogenic potential of PDGF-D in liver fibrosis. J Hepatol 2007;46(6):1064–74.

[19] Zhuo Y, et al. Modulation of PDGF-C and PDGF-D expression during bleomycin-induced lung fibrosis. Am J Physiol Lung Cell Mol Physiol 2004;286(1):L182–8.

[20] Folestad E, Kunath A, Wågsäter D. PDGF-C and PDGF-D signaling in vascular diseases and animal models. Mol Asp Med 2018;62:1–11.

[21] Sun Y, et al. A transcriptional signature of PDGF-DD activated natural killer cells predicts more favorable prognosis in low-grade glioma. Front Immunol 2021;12:668391.

[22] Gao X, Yang J, Chen Y. Identification of a four immune-related genes signature based on an immunogenomic landscape analysis of clear cell renal cell carcinoma. J Cell Physiol 2020;235(12):9834–50.

[23] Jin K, et al. Development of prognostic signature based on immune-related genes in muscle-invasive bladder cancer: bioinformatics analysis of TCGA database. Aging 2021;13(2):1859–71.

[24] He L, Yang H, Huang J. The tumor immune microenvironment and immune-related signature predict the chemotherapy response in patients with osteosarcoma. BMC Cancer 2021;21(1):581.

[25] Xiong Z, et al. Platelet-derived growth factor-D activates complement system to propagate macrophage polarization and neovascularization. Front Cell Dev Biol 2021;9:686886.

[26] Demoulin JB, Essaghir A. PDGF receptor signaling networks in normal and cancer cells. Cytokine Growth Factor Rev 2014;25(3):273–83.

[27] Ferrington DA, Gregerson DS. Immunoproteasomes: structure, function, and antigen presentation. Prog Mol Biol Transl Sci 2012;109:75–112.

[28] Franz M, et al. GeneMANIA update 2018. Nucleic Acids Res 2018;46(W1):W60–4.

[29] Jin S, et al. Inference and analysis of cell-cell communication using CellChat. Nat Commun 2021;12(1):1088.

[30] Jia X, et al. JAM-C maintains VEGR2 expression to promote retinal pigment epithelium cell survival under oxidative stress. Thromb Haemost 2017;117(4):750–7.

[31] Robador PA, et al. HIF-1-mediated up-regulation of cardiotrophin-1 is involved in the survival response of cardiomyocytes to hypoxia. Cardiovasc Res 2011;92(2):247–55.

[32] Bryan JM, et al. Identifying core biological processes distinguishing human eye tissues with precise systems-level gene expression analyses and weighted correlation networks. Hum Mol Genet 2018;27(19):3325–39.

[33] Muchamuel T, et al. A selective inhibitor of the immunoproteasome subunit LMP7 blocks cytokine production and attenuates progression of experimental arthritis. Nat Med 2009;15(7):781–7.

[34] Osusky R, et al. MHC class II positive retinal pigment epithelial (RPE) cells can function as antigen-presenting cells for microbial superantigen. Ocul Immunol Inflamm 1997;5(1):43–50.

[35] Eskandari SK, et al. The immunoproteasome: An old player with a novel and emerging role in alloimmunity. Am J Transpl: J Am Soc Transpl Am Soc Transpl Surg 2017;17(12):3033–9.

[36] Schmidt C, et al. Immunoproteasome inhibition impairs T and B cell activation by restraining ERK signaling and proteostasis. Front Immunol 2018;9:2386.

[37] Liu W, Spero DM. Cysteine protease cathepsin S as a key step in antigen presentation. Drug N Perspect 2004;17(6):357–63.

[38] Beswick EJ, Reyes VE. CD74 in antigen presentation, inflammation, and cancers of the gastrointestinal tract. World J Gastroenterol 2009;15(23):2855–61.

[39] Su H, et al. The biological function and significance of CD74 in immune diseases. Inflamm Res 2017;66(3):209–16.

[40] Schroder B. The multifaceted roles of the invariant chain CD74–More than just a chaperone. Biochim Biophys Acta 2016;1863(6 Pt A):1269–81.

[41] Schuld NJ, et al. Immunoproteasome deficiency protects in the retina after optic nerve crush. PLoS One 2015;10(5):e0126768.

[42] Sripathi SR, et al. Proteome landscape of epithelial-to-mesenchymal transition (EMT) of retinal pigment epithelium shares commonalities with malignancy-associated EMT. Mol Cell Proteom 2021;20:100131.

[43] Zhou M, et al. Role of epithelial-mesenchymal transition in retinal pigment epithelium dysfunction. Front Cell Dev Biol 2020;8:501.

[44] Niknami Z, et al. The association of vimentin and fibronectin gene expression with epithelial-mesenchymal transition and tumor malignancy in colorectal carcinoma. EXCLI J 2017;16:1009–17.

[45] Sudo T, et al. Expression of mesenchymal markers vimentin and fibronectin: the clinical significance in esophageal squamous cell carcinoma. Ann Surg Oncol 2013;20(Suppl 3):S324–35.

[46] Buechler MB, et al. Cross-tissue organization of the fibroblast lineage. Nature 2021;593(7860):575–9.

[47] Ramos de Carvalho JE, et al. Complement factor C3a alters proteasome function in human RPE cells and in an animal model of age-related RPE degeneration. Invest Ophthalmol Vis Sci 2013;54(10):6489–501.

[48] Ahmado A, et al. Induction of differentiation by pyruvate and DMEM in the human retinal pigment epithelium cell line ARPE-19. Invest Ophthalmol Vis Sci 2011;52(10):7148–59.

[49] Peng S, et al. Claudin-3 and claudin-19 partially restore native phenotype to ARPE-19 cells via effects on tight junctions and gene expression. Exp Eye Res 2016;151:179–89.

[50] Alexander JJ, Hauswirth WW. Adeno-associated viral vectors and the retina. Recent Adv Retin Degener 2008;613:121–8.

[51] Zhang F, et al. VEGF–B is dispensable for blood vessel growth but critical for their survival, and VEGF–B targeting inhibits pathological angiogenesis. Proc Natl Acad Sci USA 2009;106(15):6152–7.

[52] Butler A, et al. Integrating single-cell transcriptomic data across different conditions, technologies, and species. Nat Biotechnol 2018;36(5):411–20.

[53] Korsunsky I, et al. Fast, sensitive and accurate integration of single-cell data with Harmony. Nat Methods 2019;16(12):1289–96.

[54] Yu G, et al. clusterProfiler: an R package for comparing biological themes among gene clusters. OMICS 2012;16(5):284–7.

[55] Yu G, et al. DOSE: an R/Bioconductor package for disease ontology semantic and enrichment analysis. Bioinformatics 2015;31(4):608–9.

[56] Shannon P, et al. Cytoscape: a software environment for integrated models of biomolecular interaction networks. Genome Res 2003;13(11):2498–504.

[57] Van de Sande B, et al. A scalable SCENIC workflow for single-cell gene regulatory network analysis. Nat Protoc 2020;15(7):2247–76.

[58] Zhou Y, et al. Metascape provides a biologist-oriented resource for the analysis of systems-level datasets. Nat Commun 2019;10(1):1523.

[59] Saelens W, et al. A comparison of single-cell trajectory inference methods. Nat Biotechnol 2019;37(5):547–54.